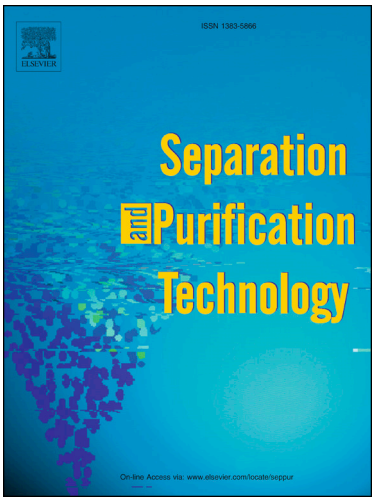

Evaluation of agarose-entrapped magnetic nanoparticles influence on protein adsorption isotherm and kinetics using nickel-iminodiacetic acid ligand

Sahar Amiri, Mohammad Reza Mehrnia, Sepide Sobhanifard, Fatemeh Pourasgharian Roudsari, Seyyed-Nezamedin Hoseini

PII: S1383-5866(17)30530-0
DOI: http://dx.doi.org/10.1016/j.seppur.2017.07.030
Reference: SEPPUR 13887

To appear in: *Separation and Purification Technology*

Received Date: 15 February 2017
Revised Date: 14 May 2017
Accepted Date: 12 July 2017

Please cite this article as: S. Amiri, M. Reza Mehrnia, S. Sobhanifard, F. Pourasgharian Roudsari, S-N. Hoseini, Evaluation of agarose-entrapped magnetic nanoparticles influence on protein adsorption isotherm and kinetics using nickel-iminodiacetic acid ligand, *Separation and Purification Technology* (2017), doi: http://dx.doi.org/10.1016/j.seppur.2017.07.030

Evaluation of agarose-entrapped magnetic nanoparticles influence on protein adsorption isotherm and kinetics using nickel-iminodiacetic acid ligand

Sahar Amiri[a], Mohammad Reza Mehrnia[1,a], Sepide Sobhanifard[a], Fatemeh Pourasgharian Roudsari[a], Seyyed-Nezamedin Hoseini[b]

[a] *School of Chemical Engineering, College of Engineering, University of Tehran, P. O. Box: 11155-4563, Tehran, Iran*

[b] *Pasteur Institute of Iran (IPI), No. 69, 12th Farwardin Ave, P.O. Code: 1316943551, Tehran, Iran*

Abstract

Employing magnetic beads for immobilized metal affinity chromatography application was studied with the approach of magnetic effects investigation. Hence, fabricated magnetic nanoparticles-carrying beads were functionalized with Ni(II)-iminodiacetic acid (IDA). BET-BJH results showed that nanoparticles affected pore sizes lower than 10nm. Therefore, the pore blockage by protein molecules is considered as an outcome of the new pore diameter in magnetic beads. In accordance, bovine serum albumin (BSA) adsorption isotherms revealed a significant difference between magnetic and nonmagnetic beaded matrices. For nonmagnetic beads, adsorption isotherm followed Langmuir model. However, one step increase in adsorption isotherm for initial BSA concentration from 0.5mg/ml to 0.8mg/ml was observed on magnetic beads due to pore blockage by proteins. BSA Adsorption kinetics on beads was found to follow the assumptions of an intraparticle diffusion-controlled pseudo-second order mechanism, with higher adsorption rate constants at lower adsorbate concentrations.

[1] Corresponding author: Tel: (98-21) 61112184, Fax: (98-21) 6695 7784. Email: mmehrnia@ut.ac.ir

Furthermore, though the same IDA density on both non/magnetic beads, presence of magnetic nanoparticles reduced the required equilibrium time (up to 60min), the saturation path of BSA adsorption breakthrough curves, dynamic binding capacity and the number of theoretical plates. It is concluded that magnetic characteristic of composite agarose adsorbent carrying Fe_3O_4 nanoparticles affects protein's conformation. Thus, BSA travel toward ligand is enhanced and sped up.

Keywords: Agarose beads; Fe_3O_4 nanoparticles; Magnetization; Ni (II)-iminodiacetic acid; protein adsorption properties

1. Introduction

Despite many efforts, purification of peptides and proteins, more than laboratory scales, is remaining as a big challenge. Since 2000, efforts have been done in the field of separation by immobilized metal affinity chromatography (IMAC) method including employing different metal ions, comparison of new chelating agents with old ones, and purification of a variety of proteins such as immunoglobulins [1,2] and recombinant proteins [3-5]. Also, histidine tag proteins are effectively purified using IMAC [6, 7]. This is based on recognition of affinity for metal ions such as zinc, copper, nickel, and cobalt which are immobilized on a matrix for binding to histidine and cysteine in protein structure [8]. Generally, IMAC has four parts [9, 10]:

-the matrix (like agarose), on which different chelates can be attached via spacer arms,

-chelating agents (like iminodiacetic acid (IDA) and nitrilotriacetic acid (NTA)) which can efficiently adsorb metal ions [6, 9, 10],

-metal ions (like Ni^{2+}),

-biological macromolecules (like proteins) owning histidine groups.

Recently, using nanoparticles in various applications is expanding [11-14]. Using metal nanoparticles in adsorbents exhibit considerable physical and chemical properties [13]. Unlike other chelates used in IMAC, IDA as a chelating agent, can easily attach to the support and does not require a complicated synthesis. In this work, Ni(II)-IDA was coupled to either magnetic (containing Fe_3O_4 nanoparticles) or nonmagnetic 6%-agarose beads to make affinity matrices. To date, fast and simple separation procedure of magnetic beads, using magnets, has been known as the main advantage of employing such beads. However, here we look for a more logical reason to choose between magnetic or nonmagnetic beads as the more efficient matrices for use in affinity chromatography.

Based on the literature review, the data on characterization of different fabricated non/magnetic beads is restricted to the research; thus, results are not statistically comparable. In other words, particle size distribution, porosity, ligand density, and magnetic nanoparticle properties differ from research to research.

In this work, both magnetic and nonmagnetic 6%-agarose beads were prepared in a way to have similar size distribution and ligand density. So, the only difference between the two bead types was magnetization. Afterwards, functionalized beads were studied in bovine serum albumin (BSA) adsorption process procedure, as the model protein. The efficiency of two adsorbents was studied by comparing maximum and dynamic binding capacities, and number of theoretical plates (N_t).

2. Experimental

2.1. Chemicals and beads characterization

BSA, epichlorohydrin (ECH), IDA, nickel(II)chloride, and other chemicals used in this work for preparation of sorbents were purchased from Sigma-Aldrich and used without additional

purification. The non/magnetic 6%-agarose beads with 50-150 µm diameters were prepared as previously described in our latest works [15, 16]. For magnetic beads as described before Fe_3O_4 nanoparticles were used in amounts of 0.48 g per 20 ml of aqueous solution. The magnetic response of the beads was evaluated by attracting them with a permanent magnet (200 mT). Accordingly, each time a permanent magnet was placed next to the container [15].

2.2. IDA-coupled beads preparation

First of all, epoxy activation of beads was done based on Porath method [17]. Afterwards, IDA was immobilized on beads as described in our previous work [18]. Fourier transform infrared (FTIR) spectroscopy (BRUKER: TENSOR 27, Germany) was used to verify the presence of IDA molecules immobilized on the non/magnetic beads. Finally, immobilized IDA density was measured by elemental analysis (Thermo finnigan Eager series EA1114).

2.3. Nickel ion immobilization and determination on magnetic and nonmagnetic 6%-agarose bead

A 50 mM Ni(II) solution was prepared in a 25 mM buffer phosphate, pH 7. Then 15 ml of IDA-modified beads were added to this solution and stirred for 2 hours at room temperature. Consequently, nickel ions were immobilized on the beads. Then, beads were washed using 25 mM buffer phosphate (pH 7) to remove the unbounds of Ni(II). Changing beads color to green was an indicator for nickel ions adsorption on beads. Finally, immobilized Ni density was measured by inductively coupled plasma (ICP) (VARIAN VISTA-PRO).

2.4. BSA adsorption on IMAC non/magnetic microspheres

In order to investigate the effect of magnetism on characteristics of the fabricated functionalized beads, BSA adsorption kinetics and isotherms were determined through adsorption experiments. For this purpose, BSA (0.5, 1, 2, and 4 mg/ml) was prepared in 0.1

M phosphate buffer solution (pH=7), and 15 ml of magnetic/nonmagnetic Ni(II)-IDA-coupled 6%-agarose beads were added to each solution. The mixtures were stirred at 100 rpm at room temperature till reaching equilibrium. At specific intervals, microspheres were separated and the supernatant was analyzed by spectrophotometer (at 280 nm) to measure protein concentration.

Two kinetics models were applied to describe the mechanism and rate of BSA physical adsorption on either magnetic or nonmagnetic affinity beads. It was assumed that adsorption follows one of the pseudo-second or pseudo-first order rate equations. The pseudo-first order equation is generally expressed as [19]:

$$\log(q_e - q_t) = \log q_e - \left(\frac{k_{ads}}{2.303}\right) t \qquad \text{eq. (1)}$$

Where, q_e and q_t are, respectively, the masses of BSA adsorbed at equilibrium at time t, t is time, and k_{ads} is the specific rate constant in min^{-1}.

The pseudo-second order equation is given in Eq. (2) as [20]:

$$\frac{dq_t}{dt} = k_{ads}(q_e - q_t)^2 \qquad \text{eq. (2)}$$

Integrating Eq. (2) gives:

$$\frac{t}{q_t} = \frac{1}{h} + \frac{1}{q_e}.t \qquad \text{eq. (3)}$$

Where $h = k_{ads} q_e^2$ (mg g^{-1} min^{-1}) can be regarded as the initial adsorption rate.

Furthermore, the static binding capacities of magnetic and nonmagnetic affinity adsorbents were determined through partition equilibrium studies. Based on the generated Langmuir isotherms ($C_{ads} = \frac{C_m \times C_{eq}}{K_d + C_{eq}}$ eq. (4)) [21], maximum adsorption capacities (C_m) and dissociation constants (K_d) of BSA with affinity ligand were calculated. In equation 4, C_{eq} and C_{ads} are the aqueous phase protein concentration and the adsorbed protein density in equilibrium, respectively.

To investigate these models, coefficient of determination (R^2) as well as root mean square error (RMSE) was used:

$$RMSE = \sqrt{\frac{1}{p}\sum_{i=1}^{p}(q_e - q_c)^2} \qquad \text{eq. (5)}$$

Where, q_c is calculated from model, q_e is taken from experiment, and p is the number of experiment parameters. It is known that if RMSE is lower, the model prediction will be more accurate [22].

2.5. Dynamic BSA separation

Breakthrough behavior of the affinity adsorbents was studied using packed bed columns of 14 mm internal diameter. In all experiments the column was loaded with 7 ml of beads at room temperature. After stabilizing beads with binding buffer, protein solution (2 mg/ml) was pumped into the column in 1 ml/min flow rate. The liquid flow rate was kept constant during dynamic adsorption experiments. Protein samples were collected in fractions (1.0 ml per fraction) from column outlet throughout operation. Effluent protein concentration was determined by spectrophotometer at 280 nm. DBC (q10%) was calculated from breakthrough curves according to Hardin et al. (2009) [23].

2.6. Elution of protein

After reaching column saturation, each column (loaded with 7 ml of beads as in section 2.5) was washed with adequate binding buffer in order to remove unbound protein molecules from columns. In the meantime, the adsorbed BSA on beads was quite stable; hence, no bound BSA was washed out during this stage. Subsequently, bound BSA was eluted from each column using elution buffer (100 mM imidazole in 100 mM phosphate buffer, pH=7). BSA elution happened due to imidazole presence and its competition with histidine for

binding to the ligand. The final BSA concentration within the desorption medium was determined spectrophotometrically at 280 nm.

In order to compare the separation efficiency of the two magnetic and nonmagnetic columns, number of theoretical plates (N_t) was calculated using eq. (6) [24];

$$N_t = 5.54\left(\frac{t_r}{W_{1/2}}\right)^2 \qquad \text{eq. (6)}$$

Where, t_r is the retention time of the BSA, and $W_{1/2}$ is the width of the peak at one half the maximum height.

3. Results and discussion

3.1. Characterization of IDA-coupled non/magnetic agarose beads

Morphological characteristics of the fabricated magnetic and nonmagnetic agarose beads were investigated by optical microscopic photographs (Figure 1 (a and b)). As shown in Figure 1 (a and b) the prepared beads are sphere. In Figure 1-a, fine black dots represent the entrapped magnetic particles within the microspherical beads. The Fe_3O_4 nanoparticles are dispersed within the aqueous droplets during bead synthesis. Thus, nanoparticles entrapment and hydrogel bead polymerization occured simultaneously.

Figure 1- (a) Optical photograph of magnetic and (b) nonmagnetic agarose beads and (c) FT-IR spectrum for non/magnetic 6%-Agarose, Fe_3O_4 nanoparticles and IDA coupled non/magnetic 6%-Agarose

Nanoparticles aggregation may take place in aqueous solution before polymerization. Several studies reporetd coagulation and/or aggregation of free uncouted nanoparticles in presence of

ions in aqueous solutions [25, 26]. Therefore, magnetic particles may be entrapped within hydrogel network either in the form of aggregates or discrete nanoparticles.

The magnetization of beads which hold entrapped magnetic particles was measured [15]. Maximum amount of magnetization for prepared beads was 12 EMU/g beads. It was found that a 2000 G magnetic field is adequate for exciting all of the dipole moments presented in 1.0 g of magnetic agarose beads. Thus, our fabricated magnetic agarose beads can easily get caught in magnetic separation. Such a strong magnetic characteristic is an important designing parameter for beads application in a magnetically stabilized fluidized bed or magnetic filtration [27].

Additionally, magnetization amount of the fabricated magnetic agarose beads maintained unchanged after four months. Consequently, it can be concluded that nanoparticles leakage from the agarose pores is quite negligible due to well entrapment within the network. This indicates the stability of the magnetic characteristic of Fe_3O_4-containing agarose beads as described in our latest work [15].

The FTIR analysis of magnetic and nonmagnetic 6%-agarose beads was performed before and after IDA immobilization on beads. The obtained spectra are shown in Figure 1-c. For non/magnetic agarose beads, the wide peak at ~3450 cm^{-1} belongs to the stretching vibration of O–H groups; and, stretching vibration of C–H groups' peak is seen at 2950 and 2850 cm^{-1}. Also, the peak around 1065cm^{-1} is assigned to the C–O stretching vibration from the primary alcohol in agarose. Furthermore, magnetic beads spectrum reveals absorption at 590 cm^{-1} which belongs to ferrous. Diagrams of non/magnetic beads before and after IDA immobilization vary. The spectra of both bead types before ligand immobilization do not exhibit any adsorption at wave number of 1674 cm^{-1} which belongs to IDA carboxylate

groups. While this peak appeared in the spectra of both types of beads after IDA immobilization. Therefore, it is concluded that IDA immobilization on beads was successful.

3.2. Ligand density

Accurate determination of ligand c/oncentration is critical since ligand density is an important factor in determining the binding capacity and separation efficiency for affinity chromatography. Theoretically, IDA and Ni(II) ions form a chelate complex with a 1:1 stoichiometric portion. Thus, it was assumed that same number of moles of IDA and Ni(II) ions was immobilized on matrices [28]. The IDA density on both magnetic and nonmagnetic beads was measured using elemental analysis. The data is represented in Table 1.

Table 1- Elemental analysis data of agarose and IDA-immobilized magnetic and nonmagnetic agarose beads (The results are based on 1 g of dried beads).

Stoichiometrically, the number of moles of N equals the number of moles of immobilized IDA on beads. Based on the data (Table 1), atoms of N form 0.15-0.20% composition of IDA-coupled non/magnetic 6%-agarose beads, whereas no nitrogen element is found in unfunctionalized beads [29]. On the other hand, 1 ml of filtered, and then freeze dried, nonmagnetic beads weighed almost 0.60 ± 0.03 mg, while 1 ml of freeze dried magnetic beads weighed almost 0.75 ± 0.04 mg. As a result, IDA densities on magnetic and nonmagnetic beads were 11.4 and 11.9 mg/ml, respectively. Based on ICP analysis and determination of Ni ions on beads the equality of Ni moles and IDA moles was proven.

Based on statistical analysis and Table 1, the ligand densities of both magnetic and nonmagnetic beads were almost the same (p value=0.4). On the other hand, based on BET-BJH analysis (Table 2), specific surface areas of magnetic and nonmagnetic beads were 5.93 m^2g^{-1} and 0.61 m^2g^{-1}, respectively. This indicates that though specific surface area of beads

increased in presence of nanoparticles, same functionalization degree took place on the surface of both types of beads. Therefore, IDA ligand density had no considerable difference on any of the two bead types. In other words, the only influential parameter affecting the adsorption characteristics of magnetic and nonmagnetic beads was the presence of Fe_3O_4 nanoparticles in magnetic beads' matrix. Thus, magnetism effect on bioseparation characteristics of discussed matrices can be evaluated as the only influential parameter.

Table 2. BJH pore size distribution for magnetic and nonmagnetic beads

3.3. Affinity adorption capacity

Affinity adsorption capability of Ni(II)-IDA-coupled magnetic and nonmagnetic beads were studied and compared using BSA adsorption kinetics and isotherms. Prior to that, nonspecific BSA adsorption was investigated too. Results are represented and discussed in the following.

3.3.1. Main contribution of different components in the protein adsorption

Nonspecific adsorption of BSA to each component of sorbent was tested by carrying out the static adsorption experiments, using unfunctionalized non/magnetic beaded gel, as well as nanoparticles directly.

Though virgin magnetic nanoparticles showed 1.38 mg BSA adsorbed per 1 g of particles, unfunctionalized magnetic beads had very negligible nonspecific adsorption (0.09 mg BSA/g drained bead). Hence, it is clear that by capturing Fe_3O_4 nanoparticles inside agarose network the nonspecific affinity of nanoparticles was suppressed. It is concluded that BSA adsorption on functionalized beads is the result of ligand's affinity- not the nanoparticles- for the protein.

3.3.2. Protein adsorption kinetics by Ni-IDA-coupled non/magnetic agarose beads.

Adsorption kinetics of BSA on magnetic and nonmagnetic Ni(II)-IDA-coupled 6%-agarose beads is shown in Figure 2. The required time for reaching equilibrium in BSA solution was

170 and 110 minutes for nonmagnetic and magnetic beads, respectively. Also, the data in Table 2 shows that the number of mesopores increased in magnetic beads. Apparently, increasing the number of mesopores of beads (2 nm< r <50 nm) resulted in raising the protein's chance to approach the affinity ligand.

Based on the results, nanoparticles enhanced the mass transfer through pores. Thus, the time taken to reach the static capacity is faster for magnetic beads contrary to nonmagnetic ones which possess small pores. Same results are reported by [30].

Figure 2. Adsorption kinetic for Ni(II)-IDA-coupled 6%-agarose (a) nonmagnetic, and (b) magnetic beads

The parameters k_{ads} and q_e were obtained from the plots of log $(q_e - q_t)$ and t/q_t versus t for each of the two kinetic models (equations 1 and 3). The coefficient of determination (R^2) was chosen as the error function for the kinetic model analysis. For the pseudo-first order kinetic model R^2 was smaller than that of the pseudo-second order model. Results reveal that for all four defined concentrations, pseudo-second order model can explain the data of magnetic and nonmagnetic beads more accurately (lower RMSE and $R^2 > 0.98$) compared to pseudo-first order model.

As shown in Table 3, adsorption rate coefficient found to be higher at lower adsorbate concentration. This implies that at high concentrations of BSA (> 1 mg BSA/ml), protein molecules caused limitations for each other to reach the affinity ligand. For BSA concentrations less than 1 mg/ml, smaller adsorption coefficients were achieved. This indicates that BSA concentration for enhanced diffusion and stabilization on ligand must be low.

Also, the specific rate constants for adsorption of BSA onto magnetic beads were found to be greater than nonmagnetics (Table 3). This outcome could be attributed to surface roughness of magnetic beads [24]. Based on the results obtained in this study, magnetic 6%-agarose beads are better adsorbents than nonmagnetic ones.

Table 3- R^2, RMSE, k_{ads} of pseudo 1st and 2nd order kinetics with q_e for 2nd order kinetics model.

3.3.3. Static adsorption isotherm of BSA on prepared Ni(II)-IDA-coupled beads

BSA adsorption isotherms for both magnetic and nonmagnetic 6%-agarose beads are represented in Figure 3.

Figure 3. Adsorption isotherms for prepared beads.

Contrary to nonmagnetic beads' adsorption isotherms which follows Langmuir model, a sudden step change is seen in adsorption isotherm of magnetic beads at initial BSA concentration of 0.5-0.8 mg/ml. As mentioned previously, both bead types carry similar ligand densities. Also, as explained in section 3.1, magnetic nanoparticles can not directly adsorb BSA molecules due to entrapment within beads [see also 15]. Therefore, the only influential parameter causing this observation is porosity alteration of magnetic beads.

In the current study, the overall effect of Fe_3O_4 nanoparticles entrapped within agarose beads is subjected to investigation as a magnetic bed. In other words, magnetic matrix (lots of beads) influence on BSA adsorption isotherm and kinetics was studied regardless of protein diffusion and adsorption within single pores. Protein molecules diffusion in a pore with a complex structure which may be affected by entrapped nanoparticles location and amount needs to be studied in the future researches.

Based on our latest work [15], though encapsulated Fe_3O_4 nanoparticles in agarose beads could not directly participate in BSA adsorption, and there is a strong static quenching and primary electrostatic interaction between encapsulated magnetic nanoparticles and BSA.

Based on BET-BJH analysis (Table 2), magnetic 6%-agarose beads have more pores of $\leq 10nm$ radius than nonmagnetic ones. It is believed that pores larger than 30nm turned into small ones ($\leq 10nm$) due to entrapped nanoparticles, discrete or aggregated, within the network. On the other hand, BSA molecules can block pores of $\leq 10nm$. This phenomenon was introduced by Rorre et al. [30] and can well describe the stepped shape of the adsorption isotherm.

Considering the data from magnetic adsorption isotherm together with BSA-caused pore blockage [30], it is implied that at initial BSA concentrations up to 0.5 mg/ml, the protein molecules did not completely penetrate through the particles; thus, they were preferentially adsorbed near the outer surface of the magnetic beads. However, increasing BSA initial concentration to 0.8 mg/ml resolved the resistance against intraparticle diffusion of protein molecules into the porous matrix.

In contrast, above 0.8 mg/ml BSA initial concentration, the flux of proteins was high; thus, proteins penetrated deep into the interior porous matrix until the pores were finally clogged. In this case the proteins loaded into the bead more uniformly; hence, higher adsorption capacity was achieved.

Based on static adsorption data, Langmuir coefficients of Eq. (4) were calculated for each bead type. The results are presented in Table 4. As seen, the maximum adsorption capacities (C_{max}) of Ni(II)-IDA-coupled magnetic and nonmagnetic agarose beads were achieved 19.00 and 12.14 mg/mL, respectively. Statistical analysis showed significant increase in C_{max} of

magnetic beads (p-value<0.01). Accordingly, higher adsorption capacity of magnetic beads was caused by magnetism effect on BSA orientation in the vicinity of ligand [15].

Though encapsulated Fe_3O_4 nanoparticles in agarose beads did not directly participate in BSA adsorption (section 3.3.1), their presence in the matrix affected secondary structure and conformation of BSA when approaching towards magnetic matrix. As a result, binding BSA molecules to ligands was enhanced. Comparably, positive effect of magnetic nanoparticles on BSA conformation, and hence, increasing the amount of BSA adsorption on affinity ligand of cibacron blue F3GA was observed in our previous study, too [15]. Accordingly, it can be concluded that this positive effect of magnetism on protein conformation enhances protein purification capacity of magnetic agarose beads.

3.3.4. Dynamic adsorption of BSA on Ni(II)-IDA-coupled beads, Protein breakthrough behavior

Breakthrough experiment is a practical chromatographic approach to examine the efficiency of adsorbents. Figure 4 presents breakthrough curves of BSA during binding to the adsorbents in the packed bed column at 1 ml/min flow rate. The dynamic adsorption capacity of magnetic 6%-agarose beads (1.71 mg/mL) was significantly higher than that of nonmagnetic ones (0.85 mg/mL). The same effect for Fe_3O_4 presence was observed on dynamic adsorption capacity of magnetic agarose beads in previous studies [15].

Figure 4. BSA breakthrough curves at 1 ml/min flux.

3.3.5. Number of theoretical plates (N_t)

As described in section 2.6, ligand-bound protein molecules were eluted from each packed column of either magnetic or nonmagnetic adsorbents. Results of elution step for Ni(II)-IDA-coupled non/magnetic 6%-agarose beads are shown in Figure 5.

Figure 5. Elution as the function of matrix composition for non/magnetic 6%-agarose

As seen in Figure 5, the maximum height in the elution peak for magnetic and nonmagnetic agarose beads is achieved at 3.48 mg BSA/ml and 2.50 mg BSA/ml, respectively. Regarding the area under the elution peak, adsorption capacity for each 1 ml of bed is 5.32 mg BSA and 2.63 mg BSA, for magnetic and nonmagnetic packed beds, respectively.

In order to compare the efficiency of the two columns, N_t for magnetic and nonmagnetic packed beds was calculated according to eq. (6). The data is presented in Table 4. Smaller N_t represents the existence of narrow peaks in elution curves and more efficient protein separation. N_t for the columns of magnetic and nonmagnetic agarose beads were 9.8 and 8.2, respectively. In other words, column efficiency of IMAC magnetic matrix was higher than nonmagnetic packed bed with same ligand densities and operation conditions.

Table 4- N_t and Langmuir coefficients for magnetic and nonmagnetic beads

4. Conclusion

As stated previously, this work mainly focused on evaluating magnetism effect on bioseparation characteristics of magnetic Ni(II)-IDA-coupled 6%-agarose beads. Magnetic nanoparticles increased surface area and the number of mesopores of magnetic beads but this increase did not have effect on functionalization degree and Ni(II)-IDA coupling on magnetic beads. Therefore, it was concluded that magnetic nanoparticles did not allow the activation reaction to progress as much that of nonmagnetic beads; thus, same ligand densities were achieved for both bead types.

Afterwards, BSA adsorption on functionalized magnetic and nonmagnetic beads was investigated. Kinetics of the adsorption for both magnetic and nonmagnetic beads was found to be based on assumptions of an intra-particle diffusion-controlled pseudo-second order

mechanism, with higher adsorption rate constants at low adsorbate concentrations. Furthermore, static adsorption isotherms, besides kinetics data, revealed that magnetization affected C_{max} and adsorption kinetics significantly. Therefore, C_{max} for magnetic samples increased while the time needed to reach equilibrium decreased about 60 minutes.

Also, dynamic BSA adsorption analysis was performed for both bead types in packed columns. Elution peak for magnetic 6% Ni(II)-IDA agarose beads was 28 ml. Comparing dynamic performance of the two columns showed that Ni(II)-IDA functionalized magnetic matrix was more efficient than nonmagnetic bed with same ligand densities and operation conditions. Apparently, magnetic beads can be used not only in fluidized and expanded beds but also in packed beds. This will increase proteins separation efficiency.

Conflict of interest

The authors declare that they have no conflict of interest.

References

[1] S.Vancan, E. A. Miranda, S. M. A. Bueno, IMAC of human IgG: studies with IDA-immobilized copper, nickel, zinc, and cobalt ions and different buffer systems, Process biochemistry, 37 (6), (2002), 573-579.

[2] M.B. Ribeiro, M. Vijayalakshmi, D.T. Balvay, S.M.A. Bueno. Effect of IDA and TREN chelating agents and buffer systems on the purification of human IgG with immobilized nickel affinity membranes, J. Chromatogr. B, 86 (2008), 64-73 .

[3] N.El Kadi, N. Taulier, J. Y. Le Huérou, M. Gindre, W. Urbach, I.Nwigwe, P. C. Kahn, M. Waks. Unfolding and Refolding of Bovine Serum Albumin at Acid pH: Ultrasound and Structural Studies, Biophysical Joun. 91, (2006), 3397–3404.

[4] H. Liu, W. J. Du, X. Y. Dong, Y. Sun, Integrative refolding and purification of histidine-tagged protein by like-charge facilitated refolding and metal-chelate affinity adsorption, J. Chromatography A, 1344, (2014), 59-65.

[5] J. T.Mooney, D. P. Fredericks and M. T.W. Hearn, Application of an IMAC cassette for the purification of N-terminally tagged proteins, Sep. Purif. Tech., 120, (2013), 265-274.

[6] E. Hochuli, W. Bannwarth, H. Do beli, R. Gentz, and D. Stuber, Genetic approach to facilitate purification of recombinant proteins with a novel metal chelate adsorbent, Biotech. 6, (1988), 1321–1325.

[7] J. Porath, J. Carlsson, I.Olsson, G. Belfrage, Metal chelate affinity Chromatography, a new approach to protein fractionation, Nature, 258 (5536), (1975), 598-599.

[8] G. S. Chaga, Twenty-five years of immobilized metal ion affinity Chromatography: past, present and future, J. Biochem. Biophys. Methods., 49(1-3), (2001), 313-334.

[9] J. Porath, Immobilized metal ion affinity chromatography, Protein Expr. Purif., 3(4), (1992), 263-81.

[10] J.Winzerling, P.Berna, J. Porath, How to use immobilized metal ion Affinity chromatography. Methods, 4(1), (1992), 4-13.

[11] O. Philippova, A. Barabanova, V. Molchanov, A. Khokhlov, Magnetic polymerbeads: recent trends and developments in synthetic design and applications,Eur. Polym. J., 47, (2011), 542–559.

[12] Z. Liao, Y. Zhang, L. Su, J. Chang and H. Wang, Application of upconversion luminescent-magnetic microbeads with weak background noise and facile separation in ochratoxin A detection, J. Nanopart. Res., 19 (2), (2017), 60-72.

[13] Q. Yang, J. Liang, H. Han, Probing the interaction of magnetic iron oxidenanoparticles with bovine serum albumin by spectroscopic techniques, J. Phys. Chem. B, 113 (2009)

10454–10458.

[14] Z.Y. Ma, Y.-P. Guan, H.-Z. Liu, Affnity adsorption of albumin on Cibacron BlueF3GA-coupled non-porous micrometer-sized magnetic polymermicrospheres, React. Funct. Polym. 66, (2006), 618–624.

[15] S. Amiri, M.R. Mehrnia, F. Pourasgharian Roodsari, Enhancing purification efficiency of affinity functionalized composite agarose micro beads using Fe_3O_4 nanoparticles, J. Chromatogr. B, 1041, (2017), 27-36.

[16] S. Amiri, M.R. Mehrnia, Preparation and characterization of controlled sized agarose beads by emulsification technique, IChEC 2015, Iran, Shiraz

[17] J.Porath, J. C. Janson, and T. Låås, agar derivatives for chromatography, electrophoresis and gel-bound enzymes i. desulphated and reduced cross-linked agar and agarose in spherical bead form, J. Chromatogr., 60, (1971), 165-177,

[18] S. Sobhani, M.R. Mehrnia, S. Amiri, Studying parameters affecting the immobilization of iminodiacetic acid on agarose beads for chromatography application, IChEC 2015, Iran, Shiraz

[19] S. Lagergren, About the theory of so-called adsorption of solution substances. kunglia srenska vertens Ka psakademiens, Handlinger, 24, (1898), 147-156.

[20] Y.S. Ho, D.A. John-Wase and C.F. Foster, Batch nickel removal from aqueous solution by sphagnum moss peat, Water Res., 29, (1995), 1327–1335

[21] Langmuir, I.The Evaporation, Condensation and Reflection of Molecules and the Mechanism of Adsorption. Phys. Rev., 8, *(*1916), 149–176.

[22] F. Gimbert, N. Morin-Crini, F. Renault, P.M. Badot, G. Crini, Adsorption isotherm models for dye removal by cationized starch-based material in a single component system: Error analysis. J.Haz. Mat., 157(1), (2008), 34- 46.

[23] A.M. *Hardin*, C. Harinarayan, G. Malmquist, A. Axén, R. van Reis, Ion exchange *chromatography* of monoclonal antibodies: effect of resin ligand density on dynamic binding capacity, J. Chromatography A. 1216, (*2009), 4366*–4371.

[24] K. H. Row, C. H. Lee, Correlation of HETP and experimental variables in preparative liquid chromatography, Korean J. Chem. Eng.,16(1), (1999), 22-27.

[25] Y. Zou, X. Wang, Z. Chen, W. Yao, Y. Ai, Y. Liu, T. Hayat, A. Alsaedi, N.S. Alharbi, X. Wang, Superior coagulation of graphene oxides on nanoscale layered double hydroxides and layered double oxides, Environmental Pollution. 2016, 219, 107-117.

[26] Y. Zou, X. Wang, Y. Ai, Y. Liu, J. Li, Y. Ji, X. Wang, Coagulation Behavior of Graphene Oxide on Nanocrystallined Mg/Al Layered Double Hydroxides: Batch Experimental and Theoretical Calculation Study, Environmental Science & Technology. 2016, 50, 3658-3667

[27] E.B. Altıntas, A. Denizli, Monosize magnetic hydrophobic beads for lysozymepurification under magnetic field, Mater. Sci. Eng. C, 29, (2009), 1627–1634.

[28] M. Zachariou, M. T. W. Hearn, Protein selectivity in immobilized metal affinity chromatography based on the surface accessibility of aspartic and glutamic acid residues, J Protein Chem, 14, (1995), 419-430.

[29] J. Li, Z. Guo, S. Zhang, X. Wang, Enrich and seal radionuclides in magneticagarose microspheres, Chem. Eng. J. 172 (2011) 892–897.

[30] G. L. Rorrer and T.-Y. Hsien, J. D. Way, Synthesis of Porous-Magnetic Chitosan Beads for Removal of Cadmium Ions from Waste Water, Ind. Eng. Chern. Res.,32, (1993), 2170-2178.

Table 1. Elemental analysis data of agarose and IDA-coupled magnetic and nonmagnetic agarose beads (The results are based on each g of dried beads).

Sample	C(%)	H(%)	N(%)
Simple agarose [29]	41.93	7.0	-0.42
IDA-coupled nonmagnetic 6%-agarose beads	40.36	5.26	0.21
IDA-coupled magnetic 6%-agarose beads	38.88	5.74	0.16

Table 2. BJH pore size distribution for magnetic and nonmagnetic beads

	magnetic 6%-agarose beads	6%-agarose bead
r_p/nm	$dV_p/dr_p \times 10^6$	$dV_p/dr_p \times 10^6$
95.27	3.7	2.5
83.877	4.8	3.3
71.895	6.6	4.5
61.314	9.0	6.1
53.044	12.1	8.2
46.13	16.0	10.9
39.006	22.5	15.3
33.814	30.3	20.6
29.501	40.8	5.5
25.548	55.9	1.5
22.072	46.2	2.2
18.936	35.7	3.2
16.287	49.1	4.5
14.125	66.5	6.3
12.244	90.5	8.9
10.651	98.6	12.348
9.2279	116.0	17.283
7.985	160.6	24.143
6.9462	127.9	32.986
6.0589	138.4	44.185
5.2867	253.9	58.859

4.6128	386.0	79.064
4.0284	572.0	104.82
3.5256	763.3	120.56
3.0877	935.7	134.17
2.7075	105.8	176.32
2.3795	170.2	228.23
2.0972	190.9	290.14
1.8527	270.8	365.4
1.6395	293.1	438.62
1.2126	241.9	543.93

Table 3. R^2, RMSE, pseudo 1st and second order k_{ads} and $C_{equilibrium}$ for second order kinetics model.

Sample	INITIAL BSA CONCENTRATION (mg/ml)	PSEUDO 1ST ORDER K_{ads}	PSEUDO 1ST ORDER R^2	PSEUDO 1ST ORDER RMSE	PSEUDO 2nd ORDER K_{ads}	PSEUDO 2nd ORDER R^2	PSEUDO 2nd ORDER RMSE	PSEUDO 2nd ORDER $C_{equilibrium}$ (mg/ml)
magnetic	4	$17.5*10^{-3}$	0.8391	1.68	$6.7*10^{-3}$	0.9914	0.99	8.98
	2	$32.2*10^{-3}$	0.9914	0.58	$14.6*10^{-3}$	0.9991	0.33	7.35
	1	$12.5*10^{-3}$	0.8870	0.91	$95.5*10^{-3}$	0.9099	0.37	3.03
	0.5	$11.2*10^{-3}$	0.7330	0.51	$14.6*10^{-3}$	0.9915	0.29	2.62
nonmagnetic	4	$5.6*10^{-3}$	0.8577	2.39	$2.6*10^{-3}$	0.9909	0.71	9.65
	2	$36.3*10^{-3}$	0.8577	0.36	$26.6*10^{-3}$	0.9987	0.42	4.03
	1	$4.6*10^{-3}$	0.6690	0.80	$84.5*10^{-3}$	0.9927	0.11	1.47
	0.5	$14.2*10^{-3}$	0.9908	0.35	$10.7*10^{-3}$	0.992	0.34	2.86

Table 4. N_t and Langmuir coefficients for magnetic and nonmagnetic beads

Sample	N_t	C_{max} (mg/ml)	k_d (mg/ml)	Molar ratio of Ni(II)-IDA to maximum adsorbed BSA concentration
Magnetic	8.27	19.00	1.95	0.52
Nonmagnetic	9.84	12.14	1.49	0.59

Figure Captions

Figure 2- Optical photograph of (a) magnetic and (b) nonmagnetic agarose beads and (c) FT-IR spectrum for non/magnetic 6%-Agarose, Fe_3O_4 nanoparticles and IDA coupled non/magnetic 6%-Agarose

Figure 2. Adsorption kinetic for Ni(II)-IDA-coupled 6%-agarose (a) nonmagnetic, and (b) magnetic beads

Figure 3. Adsorption isotherms for prepared beads.

Figure 4. BSA breakthrough curves at 1 ml/min flux.

Figure 5. Elution as the function of matrix composition for non/magnetic 6%-agarose

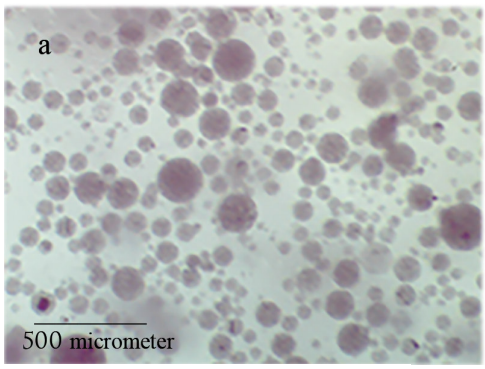

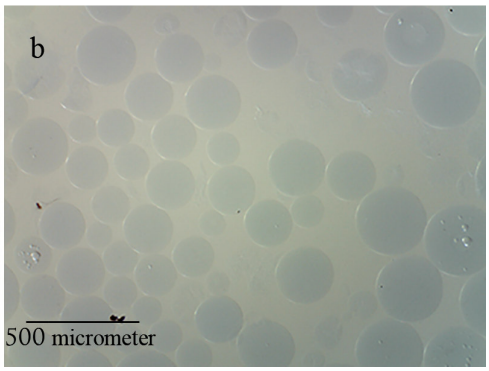

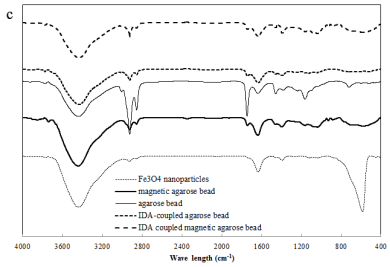

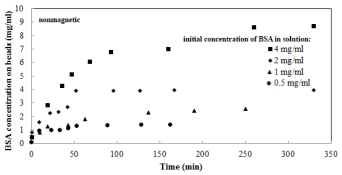

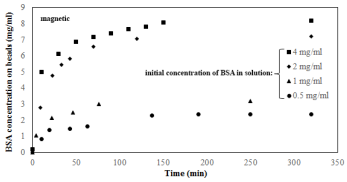

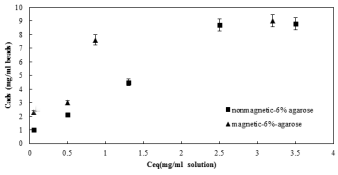

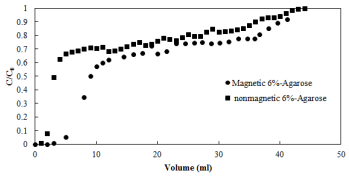

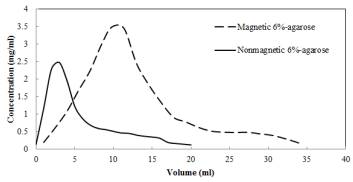

Highlights

- Investigating effects of magnetic nanoparticles on adsorption properties of beads
- Specific surface area of magnetic beads is significantly more than nonmagnetic ones
- Pore blockage in low protein concentration was seen in Ni-IDA-coupled magnetic beads
- Protein conformation and orientation were influenced by magnetic nanoparticles.
- The static and dynamic adsorption capacity was influenced by magnetic nanoparticles